Spiral rainbands as seen in numerically simulated hurricanes

Yumin Moon
Rosenstiel School of Marine and Atmospheric Science
University of Miami, Miami, Florida, USA

1. Introduction

Spiral rainbands are banded structures of convection and can be considered as clusters of individual updrafts and downdrafts where most of the strong vertical motions and associated latent heating occur. Observations (e.g. Barnes et al. 1983; Powell 1990; Hence and Houze 2008) indicate that spiral rainbands spiral radially inward in a counterclockwise direction and their upwind region is more convective while the downwind region is more stratiform (Fig. 1a). Spiral rainbands typically have three kinematic circulations: the overturning secondary circulation, the descending mid-level radial inflow, and the enhanced tangential velocity (Fig. 1b).

In recent years, steady improvements in observational and computational technology have made it possible to observe and simulate tropical cyclones with convective features on the same length scale as individual updrafts and downdrafts. This advance has made numerical simulations of tropical cyclones a very useful research tool to study the effects of spiral rainbands on the intensity and structures of hurricanes. However, whether spiral rainbands in numerically simulated hurricanes resemble those observed is not fully examined yet.

The goal of this study is to examine spiral rainbands as seen in numerically simulated hurricanes and make comparisons to observed kinematic and thermodynamic structures of spiral rainbands. Full-physics numerical simulations of Hurricane Bill (2009) are evaluated and compared to the recent observations from the Hurricane Rainband and Intensity Change Experiment (RAINEX). In addition, the conclusions of Moon and Nolan (2010, hereafter MN10), that the observed mesoscale kinematic structures associated with spiral rainbands can be explained by their mesoscale diabatic heating structures, will be evaluated.

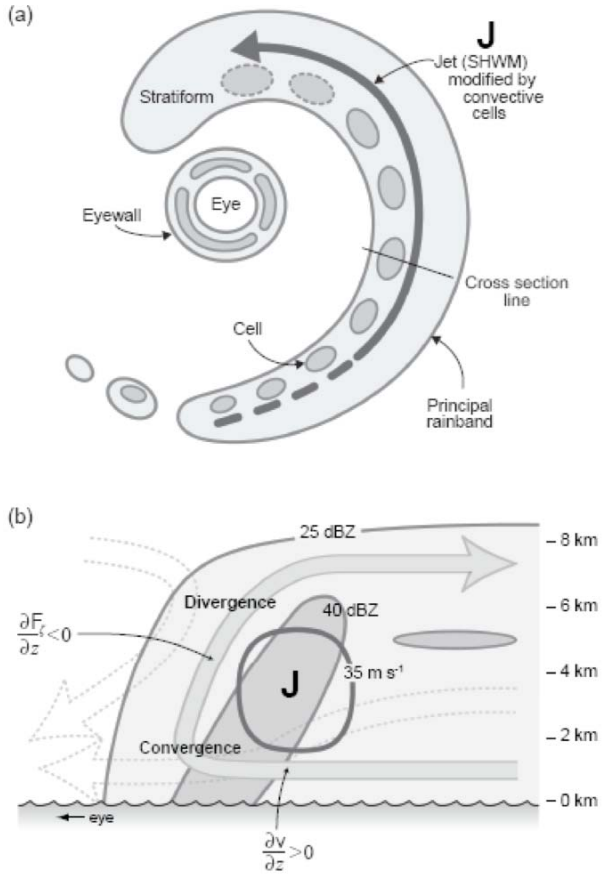

Fig. 1: Schematic diagram of precipitation and kinematic structures within spiral rainbands from Hence and Houze (2008). (a) Horizontal cross-sectional view of the conceptual spiral rainband model. (b) Radius–height cross-section along the line in (a).

2. Numerical simulation of Hurricane Bill

The simulation was performed with the Weather Research and Forecasting (WRF) model version 3.1.1. Triply nested domains are used, which have horizontal grid spacings of 9 km, 3 km and 1 km, respectively. The 3-

km and 1-km domains follow the center of the hurricane vortex. Its vertical grid has 40 levels from the surface to z = 20 km. The GFDL initial and boundary conditions are used. Standard microphysics (WSM-6 Hong et al. 2004), shortwave (Goddard; Chou et al. 1998) and longwave (Rapid Radiative Transfer Mode; Mlawer et al. 1997) radiation, and planetary boundary layer (YSU, Noh et al. 2003 and Hong et al. 2006) parameterization schemes are used for all domains. Grell cumulus parameterization is used only for the outermost 9-km domain. The evolution of Hurricane Bill is simulated from 00Z of 8/19 to 00Z of 8/22.

3. Convective-scale structures of rainbands

Many spiral rainbands develop during the numerical simulation of Hurricane Bill. On 08:20Z of 8/20, a prominent spiral rainband can be found on the eastern side of the storm (Fig. 2a). This rainband spirals radially inward from r = 100 km to 50 km. The upwind region of the rainband is more convective than the downwind region, as shown on the horizontal cross-section of vertical velocity at z = 2.58 km (Fig. 2b) To quantify this, a convective-stratiform partitioning method similar to Braun et al. (2010) is applied. A grid point was classified as convective if the surface rainfall rate is larger than 20 mm h^{-1} or if its column has vertical velocity is larger than 3 m s^{-1} or cloud liquid water of more than 0.5 g kg^{-1}. All remaining grid points with the surface rainfall greater than 0.1 mm h^{-1} were tagged as stratiform. The partitioning (Fig. 2c) indicates that convection in the upwind region is convective on the radially inward side of the rainband but stratiform on its radially outward side. In the downwind region, however, there is no clear separation between convective and stratiform types of convection.

Figure 3 shows horizontal cross-sections of radial velocity at z = 8.07 km and 1.21 km, along with the contours of vertical velocity greater than 3 m s^{-1} at z = 4.40 km. Note that z

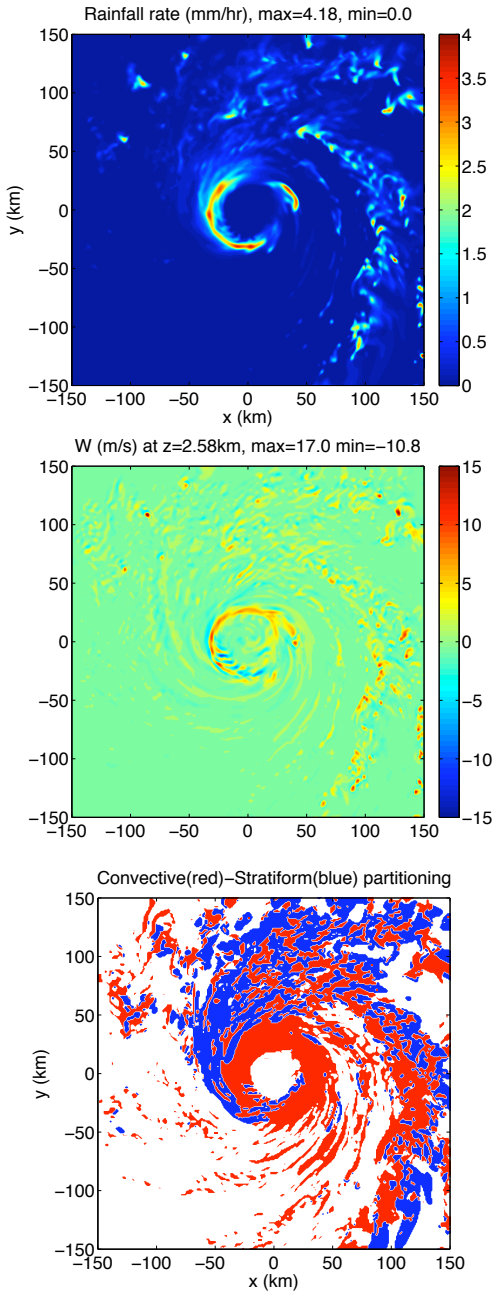

Fig. 2: (a) Surface rainfall rate; (b) The horizontal cross-section of vertical velocity at z = 2.58 km; (c) The convective-stratiform partitioning. All plots are at Aug/20 08:20Z.

= 8.07 km is well below the primary upper-level outflow of the hurricane. All horizontal motions are *storm-relative*. The figure indicates that there are upper-level radial outflow away from the rainband and low-level radial inflow toward the rainband, which are

connected by the updrafts to form the overturning circulation. Figure 4 shows the radius-height cross-sections of diabatic heating and secondary circulation (radial and vertical velocity) through the upwind, middle and downwind regions of the rainband. The diabatic heating is tilted radially outward with height in the upwind and middle regions of the rainband, but this radially outward tilt is absent in the downwind region. The descending mid-level radial inflow toward the rainband is only evident in the upwind region (near r = 155 km, from z = 3 km to 2 km). Figure 5 shows the horizontal cross section of tangential velocity at z = 4.40 km, with the black contours showing surface rainfall rate greater than 0.1 mm h^{-1}. Enhanced tangential velocity with the rainband is evident at this level (and between z = 3 km and 5 km) and stronger in the downwind region.

4. Mesoscale structures of rainbands

MN10 showed that the mesoscale kinematic rainband circulations could be recovered by imposing a hypothetical mesoscale diabatic heating that resembles the observed rainband heating (convective in the upwind region, stratiform in the downwind region, with a linear transition between them) on the hurricane-like basic-state vortex in a three-dimensional, nonhydrostatic, linear model of vortex dynamics. MN10 indicated that the overturning circulation results mostly from the convective part of the rainband and is stronger in the upwind region, while mid-level radial inflow descending to surface results from the stratiform characteristics of the rainband and is stronger located in the downwind region. The secondary horizontal wind maximum is exhibited in both convective and stratiform parts of the rainband (at the level of strong radial inflow toward the rainband), but it tends to be stronger in the downwind region.

To obtain the mesoscale structures of kinematic and diabatic heating fields, a low-pass filtering (Fourier decompositions) is applied, with the cutoff at the azimuthal wavenumber (n) of 8. Figure 6 shows the decompositions of vertical velocity at z = 2.58 km, and the upwind region has stronger rising motions thus more convective than the downwind region. Figure 7 shows the horizontal cross-sections of the filtered tangential velocity at z = 4.40 km. The n = 0-8 decomposition (Fig. 7a) captures the mesoscale kinematic structures associated with the rainband, including the enhanced tangential velocity, which is due to the asymmetric (n = 1-8, Fig. 7b) components. Although the n = 1 asymmetry due to the storm movement is removed, there are other sources contributing to the n = 1 asymmetry (Fig. 7c), such as the beta gyres and the environmental wind shear. However, the enhanced tangential velocity feature is evident in the n = 2-8 decomposition (Fig. 7d), suggesting that it is driven by internal dynamics.

Figures 8 and 9 show the horizontal cross-sections of the decompositions of radial velocity at z = 1.21 km and 8.07 km, respectively. The n = 0-8 decompositions (Fig. 8a and 9a) capture the mesoscale low-level radial inflow toward the rainband and upper-level radial outflow away from the rainband, respectively. The n = 1 component is dominant at both levels, and the regions of strong low-level radial inflow and upper-level outflow are to the left of the 850mb-to-250mb vertical wind shear vector that is directed from the northwest to the southeast (not shown).

5. Future Works

The results presented here are preliminary. Comparisons between simulated and observed spiral rainbands will continue, including the thermodynamics properties in addition to the kinematic structures. Examining the sensitivity of simulated spiral rainbands to different horizontal and vertical grid spacing, and microphysics, planetary boundary layer parameterizations is underway. The effects of

the different background flows — such as no flow, vertically uniform flow, vertically varying flow – will be examined as well.

Acknowledgements
This work was supported by the National Science Foundation grant ATM-0756308. The author would like to thank Dr. David S. Nolan and Dr. Eric D. Rappin for helpful feedbacks and technical supports.

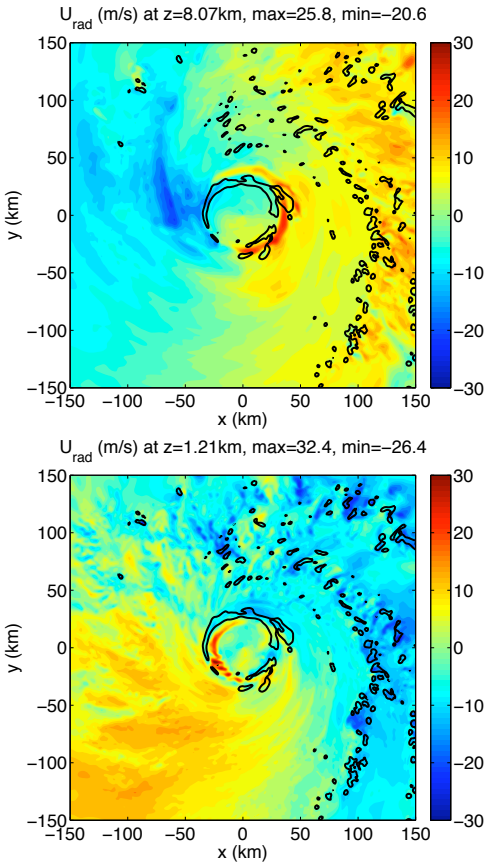

Fig. 3: Horizontal cross-sections of radial velocity at z = (a) 8.07 km and (b) 1.21 km. Solid lines show vertical velocity larger than 3 ms^{-1} at z = 4.40 km.

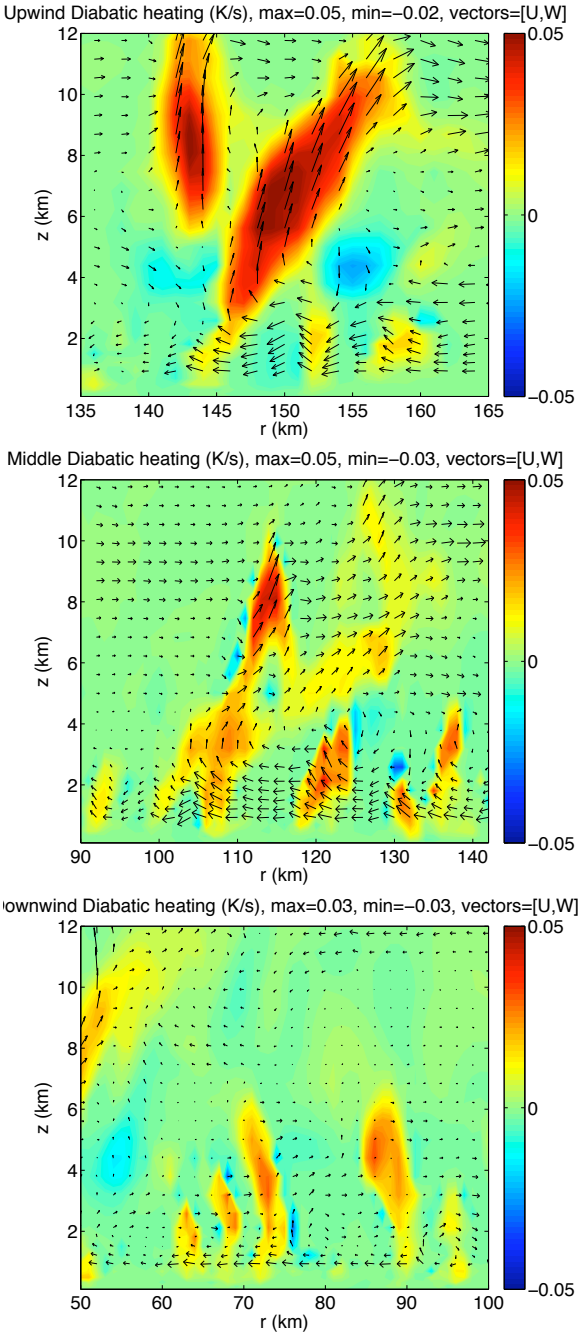

Fig. 4: Radial-height cross-sections of diabatic heating, overlaid with the vectors of radial and vertical velocity in the (a) upwind, (b) middle, and (c) downwind regions. Vectors below z = 1 km are not shown.

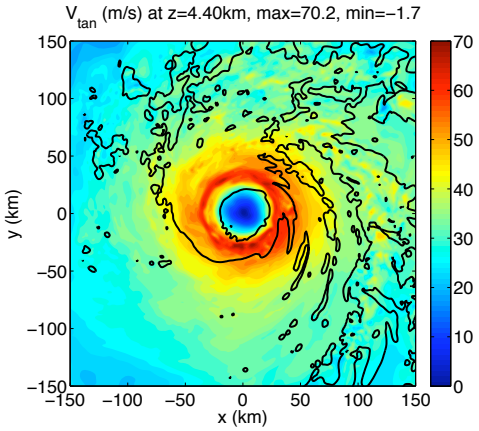

Fig. 5: Horizontal cross-section of tangential velocity at z = 4.40 km. Solid lines show surface rainfall rate larger than 0.1 mm h^{-1}.

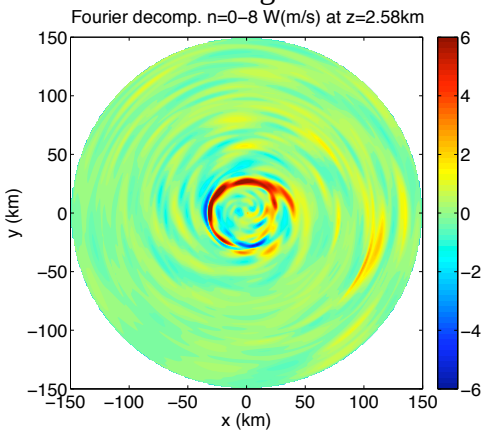

Fig. 6: The horizontal cross-section at z = 2.58 km of the Fourier decompositions (n=0-8) of vertical velocity.

References

Moon, Y., and D.S. Nolan, 2010: The dynamic response of the hurricane wind field to spiral rainband heating. *J. Atmos. Sci.*, **67**, in press.

Hence, D.A., and R.A. Houze, Jr., 2008: Kinematic structure of convective-scale elements in the rainbands of Hurricanes Katrina and Rita (2005). J. Geophys. Res., 113, D15108, doi:10.1029/2007JD009429.

Braun, S.A., M.T. Montgomery, K.J. Mallen, and P.D. Reasor, 2010: Simulation and interpretation of the genesis of Tropical Storm Gert (2005) as part of the NASA Tropical Cloud Systems and Processes Experiment. *J. Atmos. Sci.*, **67**, 999-1025.

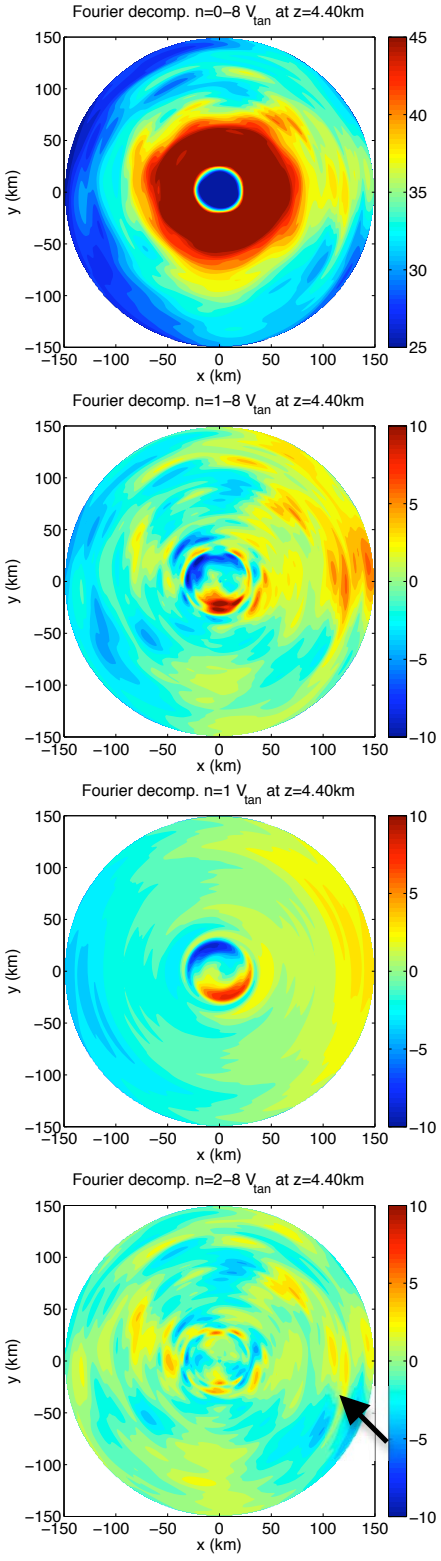

Fig. 7: Horizontal cross-sections at z = 4.40 km of the Fourier decompositions of tangential velocity, with (a) n=0-8, (b) n=1-8, (c) n=1, and (d) n=2-8.

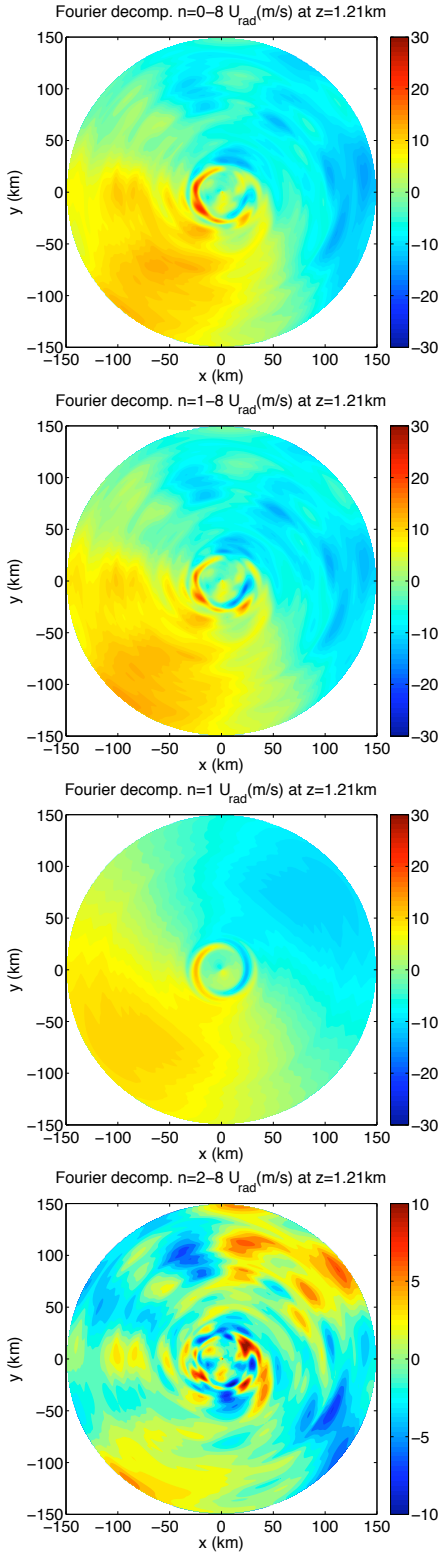

Fig. 8: Horizontal cross-sections at z = 1.21 km of the Fourier decompositions of radial velocity, with (a) n=0-8, (b) n=1-8, (c) n=1, and (d) n=2-8.

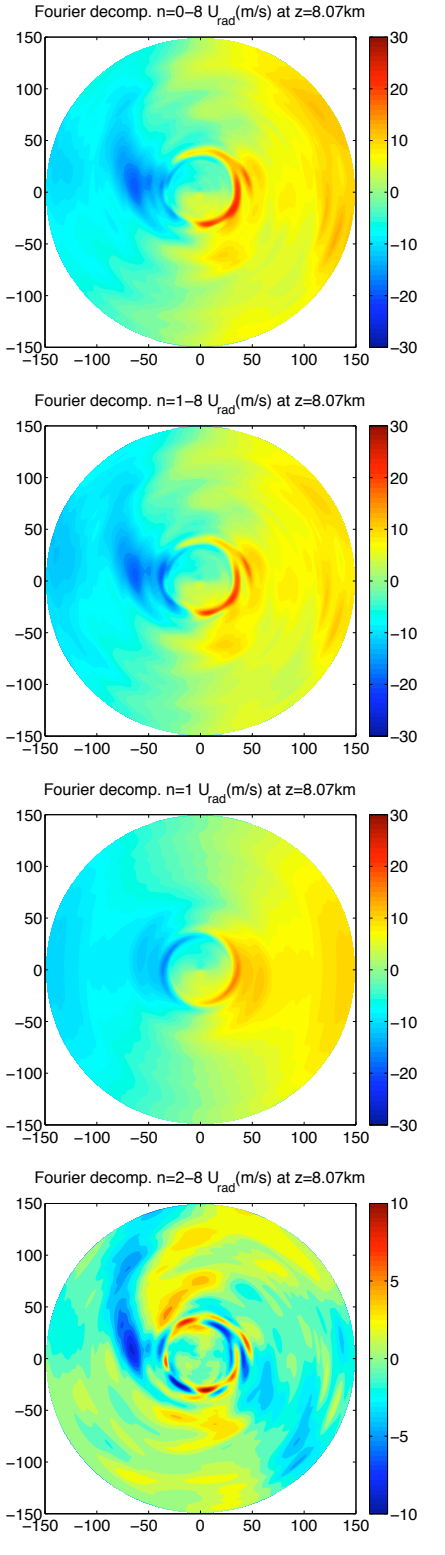

Fig. 9: Horizontal cross-sections at z = 8.07 km of the Fourier decompositions of radial velocity, with (a) n=0-8, (b) n=1-8, (c) n=1, and (d) n=2-8.